PRAMANA
— journal of
physics

© Indian Academy of Sciences

Vol. 72, No. 5
May 2009
pp. 887–902

Inter-dot coupling effects on transport through correlated parallel coupled quantum dots

SHYAM CHAND*, G RAJPUT, K C SHARMA and P K AHLUWALIA
Department of Physics, Himachal Pradesh University, Shimla 171 005, India
*Corresponding author. E-mail: shyam_hpu@yahoo.co.in

MS received 18 August 2008; revised 25 November 2008; accepted 16 December 2008

Abstract. Transport through symmetric parallel coupled quantum dot system has been studied, using non-equilibrium Green function formalism. The inter-dot tunnelling with on-dot and inter-dot Coulomb repulsion is included. The transmission coefficient and Landaur–Buttiker like current formula are shown in terms of internal states of quantum dots. The effect of inter-dot tunnelling on transport properties has been explored. Results, in intermediate inter-dot coupling regime show signatures of merger of two dots to form a single composite dot and in strong coupling regime the behaviour of the system resembles the two decoupled dots.

Keywords. Coupled quantum dots; Coulomb blockade; non-equilibrium transport; inter-dot coupling.

PACS Nos 73.23.Hk; 73.21.La; 73.63.Kv; 73.40.Gk

1. Introduction

Advances in modern technology have made possible the fabrication of nanoparticle structures called quantum dots (QDs), in which the electrons can be confined in all the three dimensions. A single quantum dot (SQD) is regarded as an artificial atom owing to its shell-like electronic structure, whereas coupled quantum dots (CQD) form molecular states and are named as artificial molecules. Transport through QDs has revealed many interesting and novel phenomena, viz. Kondo effect [1–4], Coulomb blockade (CB) [5,6], etc. using non-equilibrium Green function methods, renormalization group method and lately by exact non-perturbative non-equilibrium Bethe–Ansatz [7] and Lippman–Schwinger method [8] under different temperature regimes. Compared to SQD, the CQD are rich in physics and rapid development in the field of spintronics and quantum information processing (QIP) in quantum computing [9] have made it desirable to understand their features. Internal parameters of CQD are fully tunable thus allowing one to investigate, in a well-controlled manner, different regimes of interest. During the past years, the transport through series geometry of CQD has been studied extensively [10–12], using non-equilibrium Green function (NEGF) formalism, wherein it has been shown

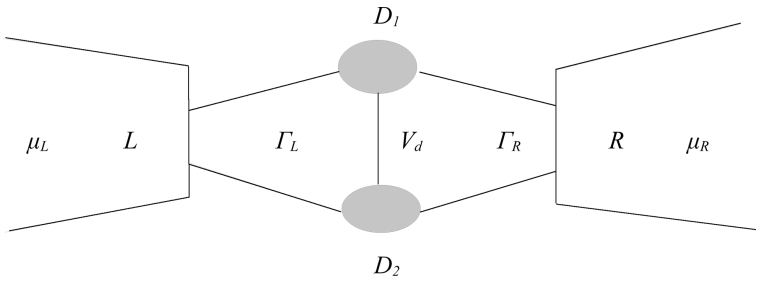

Figure 1. Schematic display of a parallel coupled quantum dot system. The two dots D_1 and D_2, are coupled to the left (L) and right leads (R) by tunnel barriers with coupling strengths $\Gamma_{\rm L}$ and $\Gamma_{\rm R}$ respectively. Here V_d is the inter-dot coupling strength and $\mu_{\rm L(R)}$, the chemical potential of the left (right) lead.

that current and differential conductance display oscillating variation with applied bias voltage. Inter-dot tunnelling splits the resonant peaks of conductance and transmission coefficient. For strong inter-dot coupling, CQD merge to form a single composite dot. In recent past, the parallel combination of CQD has also drawn a substantial attention for theoretical [13–17] and experimental [18,19] mesoscopic transport phenomena. Being more complicated than series CQD, most of the previous theoretical work on parallel CQD is either in the presence of magnetic flux [13,14] or in equilibrium condition [17] or is devoted to the interference effects. Some special geometries like side coupled dot [20] or two SQD systems placed parallel, with inter-dot tunnelling [21], have also been investigated theoretically. The phenomenon of Fano interference [17,21,22], which is not observed in series CQD, evolves in asymmetric parallel CQD due to the formation of bonding and antibonding molecular states, though, same has not been fully manifested in experiments. Recently, some theoretical work [23,24] has been done on parallel CQD in the presence of Coulomb interaction but in the absence of inter-dot tunnelling [23] or in the absence of inter-dot Coulomb interaction [24]. But non-equilibrium transport through parallel combination of CQD, in the presence of both intra- and inter-dot Coulomb interactions, in CB regime with inter-dot tunnelling included, has not been reported in theoretical work so far.

The present work deals with the transport through CQD in parallel configuration (figure 1), in CB regime using NEGF formalism. In this configuration both the dots D_1 and D_2 are symmetrically coupled through tunnel barriers to the left (L) and right (R) leads which are endowed with different electron chemical potentials $\mu_{\rm L}$ and $\mu_{\rm R}$ respectively. On-dot Coulomb interaction U and inter-dot Coulomb interaction U' among the electrons is taken into account. Experimental work on such a system [18,19] shows that $U \approx 1$ meV with single particle level spacing $\varepsilon \approx 0.05$ meV at temperature $T \approx 10$ mK (non-Kondo regime). The parameters chosen in the present theoretical work are around these values. U' is believed to be nearly 10% of U if inter-dot separation is not too large. We have assumed that each dot contains only one spin degenerate energy level so that the Kondo effect does not intervene.

Spectral and transport properties of CQD system are contained in its Green functions (GF), which have been calculated for two cases: (a) $U \neq 0$ and $U' = 0$

and (b) $U \neq 0$ and $U' \neq 0$. Detailed calculations of current, differential conductance and transmission coefficient have been presented. The role of inter-dot coupling V_d in transport properties of parallel CQD is studied over its wide range. When $V_d = 0$, the system behaves as two independent SQDs. When V_d increases, it modifies the conductance peaks and at certain point, conductance spectra show the merger of two dots to form a single composite dot which has been reported in experimental works also [18] and for strong V_d, characteristics of the system again resemble two decoupled dots. This also has been proved experimentally in some of the works [4,19]. In dealing with the calculations, three approximations have been used: (1) the central region (CQD) is weakly coupled with the environment (leads) and coupling between dots is also weak but tunable over a wide range, (2) the wide band limit, wherein coupling of leads with dots is independent of energies of electrons in leads and is assumed to be constant, (3) the Hartree–Fock approximation (HFA), to enable decoupling of higher-order GFs.

The paper has been organized as follows: Section 2 gives the model Hamiltonian and theoretical formalism. In §3, GFs of QDs have been calculated. Section 4 involves derivations of formulae. Results have been presented in §5. Finally, in §6, conclusions have been summarized.

2. Model and formalism

2.1 *Model Hamiltonian*

Energy quantization of a QD is described by single impurity Anderson model [25]. But parallel CQD, equally coupled to the leads can be described by two impurities Anderson type model, with other relevant interactions and hoppings added to its original form. For such a system it is reasonable to assume central CQD region and leads as seperate mesoscopic systems described by their respective Hamiltonians and two parts interact with each other via tunnelling process described by tunnelling Hamiltonian $H_{\rm tun}$. Model Hamiltonian is as follows:

$$H = H_{\rm leads} + H_{\rm dots} + H_{\rm tun}. \tag{1}$$

Each term in H can be described as

$$H_{\rm leads} = \sum_{k\sigma} \varepsilon_k^{\rm L} a_{k\sigma}^\dagger a_{k\sigma} + \sum_{p\sigma} \varepsilon_p^{\rm R} b_{p\sigma}^\dagger b_{p\sigma}, \tag{2}$$

where $\varepsilon_{k(p)}^{\rm L(R)}$ are energies of non-interacting free electrons in the left (right) lead, with band-like spectrum. $a_{k\sigma}^\dagger(a_{k\sigma})$ and $b_{p\sigma}^\dagger(b_{p\sigma})$ are electron creation (annihilation) operators in Heisenberg picture, of the left and right leads respectively.

$$H_{\rm dots} = \sum_{i\sigma} \varepsilon_i c_{i\sigma}^\dagger c_{i\sigma} + \sum_i U_i n_{i\uparrow} n_{i\downarrow} + \frac{U'}{2} \sum_{\sigma,\sigma'} n_{1\sigma} n_{2\sigma'}. \tag{3}$$

Here ε_i is the energy of discrete energy levels for single electron on the ith ($i = 1, 2$) dot. Here only one energy level per dot is considered. $c_{i\sigma}^\dagger(c_{i\sigma})$ are creation (annihilation) operators of electrons on dots and U_i are intra-dot Coulomb repulsion

energies of electrons in the ith dot for double occupancy with opposite spins, while U' is the inter-dot Coulomb repulsion energy and $n_{i\sigma} = c^{\dagger}_{i\sigma}c_{i\sigma}$ are electron occupation number operators.

$$H_{\rm tun} = \big(\sum_{ki\sigma} V^{\rm L}_k c^{\dagger}_{i\sigma} a_{k\sigma} + \sum_{pi\sigma} V^{\rm R}_p c^{\dagger}_{i\sigma} b_{p\sigma} + \sum_{\sigma} V_d c^{\dagger}_{1\sigma} c_{2\sigma}\big) + \text{H.C.} \tag{4}$$

where the first two terms represent tunnelling of electrons between the CQD system and the leads, with $V^{\rm L(R)}_{k(p)}$, the coupling strength of the left (right) tunnel barrier and the third term describes the hopping of electrons between two dots with inter-dot coupling strength V_d.

2.2 *Theoretical formalism*

The present case of transport through parallel CQD system connected to leads is driven by weak bias V, which destroys equilibrium state of the system, where $eV = \mu_{\rm L} - \mu_{\rm R}$ is of the order of U. Hence NEGF formalism [26–29] becomes the natural choice for the study of such mesoscopic transport. This formalism is the most suitable tool above Kondo temperature in CB regime. For any two dynamic operators A and B, the GFs namely, retarded GF, advanced GF and lesser (distribution) GF respectively are defined as

$$\langle\langle A(t_1), B(t_2)\rangle\rangle^{\rm r} = -i\theta(t_1 - t_2)\langle[A(t_1), B(t_2)]\rangle, \tag{5}$$

$$\langle\langle A(t_1), B(t_2)\rangle\rangle^{\rm a} = i\theta(t_2 - t_1)\langle[A(t_1), B(t_2)]\rangle, \tag{6}$$

$$\langle\langle A(t_1), B(t_2)\rangle\rangle^{<} = i\langle B(t_2)A(t_1)\rangle. \tag{7}$$

The symbols used in the above expressions are the same as in ref. [30], i.e. θ is the unit step function, $\langle\cdots\rangle$ represents thermal average in grand canonical ensemble and $[\cdots]$ denotes commutators for the fermionic operators. Here t_1 and t_2 are two time instants on either side of the branch in complex time contour [29] on which the theory of NEGF is constructed. In steady-state GFs depend only on the variable $t = t_1 - t_2$. Therefore, Fourier transform of $\langle\langle A(t), B(t_0)\rangle\rangle$ can be denoted as $\langle\langle A, B\rangle\rangle_\omega$. Initially, in the absence of bias voltage, dots and leads are assumed to be in their thermodynamic equilibrium characterized by their equilibrium GFs. Onset of bias lifts the system out of equilibrium and characterization of the system will be described by NEGF. To calculate these GFs, we use Dyson equations and equation of motion (EOM) method.

3. Calculations of Green functions of dots

Derivation of formulae for current and other transport properties of CQD involves all GFs defined in the previous section. But here, detailed calculations of only retarded GF of dots are presented. Calculations of other GFs (advanced and lesser) also follow similar procedure, but their calculations are not shown in the paper. Moreover, with the help of properties of NEGF and by suitable manipulations, all the formulae can be expressed in terms of retarded GF only. Here we consider two cases for the calculations of the GFs.

(a) *When $U \neq 0$ and $U' = 0$*

To calculate GFs of dots we employ EOM method [31] using the Hamiltonian defined in eq. (1) when $U' = 0$. The EOM for retarded GF of dot-1 is

$$\begin{aligned}(\omega - \varepsilon_1)\langle\langle c_{1\sigma}, c_{1\sigma}^\dagger\rangle\rangle_\omega^{\mathrm{r}} &= 1 + U_1\langle\langle n_{1-\sigma}c_{1\sigma}, c_{1\sigma}^\dagger\rangle\rangle_\omega^{\mathrm{r}} \\ &\quad + \sum_k V_k^{\mathrm{L}}\langle\langle a_{k\sigma}, c_{1\sigma}^\dagger\rangle\rangle_\omega^{\mathrm{r}} \\ &\quad + \sum_p V_p^{\mathrm{R}}\langle\langle b_{p\sigma}, c_{1\sigma}^\dagger\rangle\rangle_\omega^{\mathrm{r}} + V_d\langle\langle c_{2\sigma}, c_{1\sigma}^\dagger\rangle\rangle_\omega^{\mathrm{r}}. \qquad (8)\end{aligned}$$

The GFs $\langle\langle a_{k\sigma}, c_{1\sigma}^\dagger\rangle\rangle^{\mathrm{r}}$ and $\langle\langle b_{p\sigma}, c_{1\sigma}^\dagger\rangle\rangle^{\mathrm{r}}$ arise due to tunnelling of electrons between dots and leads. The EOM for these gives the following Dyson equations:

$$\langle\langle a_{k\sigma}, c_{1\sigma}^\dagger\rangle\rangle_\omega^{\mathrm{r}} = V_k^{\mathrm{L}*} g_k^{\mathrm{r}}(\langle\langle c_{1\sigma}, c_{1\sigma}^\dagger\rangle\rangle_\omega^{\mathrm{r}} + \langle\langle c_{2\sigma}, c_{1\sigma}^\dagger\rangle\rangle_\omega^{\mathrm{r}}), \qquad (9)$$

$$\langle\langle b_{p\sigma}, c_{1\sigma}^\dagger\rangle\rangle_\omega^{\mathrm{r}} = V_p^{\mathrm{R}*} g_p^{\mathrm{r}}(\langle\langle c_{1\sigma}, c_{1\sigma}^\dagger\rangle\rangle_\omega^{\mathrm{r}} + \langle\langle c_{2\sigma}, c_{1\sigma}^\dagger\rangle\rangle_\omega^{\mathrm{r}}), \qquad (10)$$

where $g_{k(p)}^{\mathrm{r}} = (\omega - \varepsilon_{k(p)}^{\mathrm{L(R)}} + i\delta)^{-1}$ are the single-particle GFs of free electrons in the left (right) lead. In wide band limit, only imaginary parts of $g_{k(p)}^{\mathrm{r}}$ are of importance. Similarly, the EOM for $\langle\langle c_{2\sigma}, c_{1\sigma}^\dagger\rangle\rangle_\omega^{\mathrm{r}}$ gives

$$\begin{aligned}(\omega - \varepsilon_2)\langle\langle c_{2\sigma}, c_{1\sigma}^\dagger\rangle\rangle_\omega^{\mathrm{r}} &= U_2\langle\langle n_{2-\sigma}c_{2\sigma}, c_{1\sigma}^\dagger\rangle\rangle_\omega^{\mathrm{r}} \\ &\quad + \sum_k V_k^{\mathrm{L}}\langle\langle a_{k\sigma}, c_{1\sigma}^\dagger\rangle\rangle_\omega^{\mathrm{r}} \\ &\quad + \sum_p V_p^{\mathrm{R}}\langle\langle b_{p\sigma}, c_{1\sigma}^\dagger\rangle\rangle_\omega^{\mathrm{r}} + V_d^*\langle\langle c_{1\sigma}, c_{1\sigma}^\dagger\rangle\rangle_\omega^{\mathrm{r}}. \qquad (11)\end{aligned}$$

In eqs (8) and (11), new GFs $\langle\langle n_{1-\sigma}c_{1\sigma}, c_{1\sigma}^\dagger\rangle\rangle^{\mathrm{r}}$ and $\langle\langle n_{2-\sigma}c_{2\sigma}, c_{1\sigma}^\dagger\rangle\rangle^{\mathrm{r}}$ appear due to U. The EOM of these two-particle GFs generate coupled chain of higher-order GFs. But this hierarchy is truncated using decoupling scheme [30], which involves HFA. The approximations used are

$$\begin{aligned}\langle\langle n_{1(2)-\sigma}c_{1(2)\sigma}, c_{1\sigma}^\dagger\rangle\rangle &\approx \langle n_{1(2)-\sigma}\rangle\langle\langle c_{1(2)\sigma}, c_{1\sigma}^\dagger\rangle\rangle, \\ \langle\langle n_{1(2)-\sigma}a_{k\sigma}, c_{1\sigma}^\dagger\rangle\rangle &\approx \langle n_{1(2)-\sigma}\rangle\langle\langle a_{k\sigma}, c_{1\sigma}^\dagger\rangle\rangle, \\ \langle\langle n_{1(2)-\sigma}b_{p\sigma}, c_{1\sigma}^\dagger\rangle\rangle &\approx \langle n_{1(2)-\sigma}\rangle\langle\langle b_{p\sigma}, c_{1\sigma}^\dagger\rangle\rangle.\end{aligned}$$

This decoupling scheme, valid in CB regime, ultimately reduces all the higher-order GFs containing U, in terms of $\langle\langle c_{1\sigma}, c_{1\sigma}^\dagger\rangle\rangle$ and at the same time keeps, to a reasonable extent, the qualitative features of the system and underlying physics intact. Finally, retarded GF of dot-1 becomes

$$\begin{aligned}&\langle\langle c_{1\sigma}, c_{1\sigma}^\dagger\rangle\rangle_\omega^{\mathrm{r}} \\ &\quad = \frac{Z_1}{Z_1' - Z_1\big[-i\frac{\Gamma}{2} + \big(V_d - i\frac{\Gamma}{2}\big)\big(V_d^* - i\frac{\Gamma}{2}\big)\langle\langle c_{2\sigma}, c_{2\sigma}^\dagger\rangle\rangle_{0\omega}^{\mathrm{r}}\big]}. \qquad (12)\end{aligned}$$

Here,

$$\langle\langle c_{2\sigma}, c_{2\sigma}^{\dagger}\rangle\rangle_{0\omega}^{\mathrm{r}} = \frac{Z_2}{Z_2' - Z_2\left(-i\frac{\Gamma}{2}\right)} \tag{13}$$

is the uncoupled GF of dot-2 and total coupling strength $\Gamma = \Gamma_{\mathrm{L}} + \Gamma_{\mathrm{R}}$, where

$$\Gamma_{\mathrm{L(R)}} = \sum_{k(p)} |V_{k(p)}^{\mathrm{L(R)}}|^2 g_{k(p)}^{\mathrm{r}} \tag{14}$$

represents the coupling coefficient (tunnelling rate) between left (right) lead and dots. Also for the ith dot, $Z_i = \omega - \varepsilon_i - U_i(1 - n_{i-\sigma})$ and $Z_i' = (\omega - \varepsilon_i)(\omega - \varepsilon_i - U_i)$.

(b) *When $U \neq 0$ and $U' \neq 0$*

Using eq. (1), employing the EOM technique and similar decoupling scheme, the retarded GF of dot-1 for perfect symmetric case, for which $U_1 = U_2 = U$, $\varepsilon_1 = \varepsilon_2 = \varepsilon$, and $\langle n_{i\sigma}\rangle = \langle n_{i\sigma'}\rangle = \frac{1}{2}$, is calculated as

$$\langle\langle c_{1\sigma}, c_{1\sigma}^{\dagger}\rangle\rangle_{\omega}^{\mathrm{r}} = \frac{Z}{Z' - Z\left[-i\frac{\Gamma}{2} + \left(V_d - i\frac{\Gamma}{2}\right)\left(V_d^* - i\frac{\Gamma}{2}\right)\langle\langle c_{2\sigma}, c_{2\sigma}^{\dagger}\rangle\rangle_{0\omega}^{\mathrm{r}}\right]}. \tag{15}$$

Here,

$$\langle\langle c_{2\sigma}, c_{2\sigma}^{\dagger}\rangle\rangle_{0\omega}^{\mathrm{r}} = \frac{Z}{Z' - Z\left(-i\frac{\Gamma}{2}\right)} \tag{16}$$

is the uncoupled GF of dot-2. Also, $Z = (\omega - \varepsilon - 1.5U')(\omega - \varepsilon - U - 1.5U) \times \big[(\omega - \varepsilon - 0.5U)(\omega - \varepsilon - 1.5U')(\omega - \varepsilon - U - 1.5U') + (\omega - \varepsilon - U) \times (\omega - \varepsilon - U - 1.5U')U' + \{(\omega - \varepsilon - U) + (\omega - \varepsilon - 1.5U')\}0.5UU'\big]$ and $Z' = (\omega - \varepsilon)(\omega - \varepsilon - U)(\omega - \varepsilon - 1.5U')^2(\omega - \varepsilon - U - 1.5U')^2$.

In ref. [23], the higer-order GFs generated by U' are decoupled by solving correlators self-consistently, but we have used HFA for the same.

4. Calculations of current and transmission coefficient

In order to obtain the expression for total current, we obtain the contributions from two leads seperately. The expression for current from left lead in terms of GFs can be written as [29]

$$I_{\mathrm{L}} = \frac{e}{h}\sum_{ki\sigma}\int \left[V_k^{\mathrm{L}}\langle\langle a_{k\sigma}, c_{i\sigma}^{\dagger}\rangle\rangle_{\omega}^{<} - V_k^{\mathrm{L}*}\langle\langle c_{i\sigma}, a_{k\sigma}^{\dagger}\rangle\rangle_{\omega}^{<}\right]\mathrm{d}\omega. \tag{17}$$

The GFs $\langle\langle a_{k\sigma}, c_{i\sigma}^{\dagger}\rangle\rangle^{<}$ and $\langle\langle c_{i\sigma}, a_{k\sigma}^{\dagger}\rangle\rangle^{<}$ $(i = 1, 2)$ can be calculated using Langreth analytic continuation rules [32] as

$$\langle\langle a_{k\sigma}, c^{\dagger}_{1(2)\sigma}\rangle\rangle^{<} = V^{\mathrm{L}*}_{k} g^{\mathrm{r}}_{k}\big(\langle\langle c_{1(2)\sigma}, c^{\dagger}_{1(2)\sigma}\rangle\rangle^{<} + \langle\langle c_{2(1)\sigma}, c^{\dagger}_{1(2)\sigma}\rangle\rangle^{<}\big) + V^{\mathrm{L}*}_{k} g^{<}_{k}\big(\langle\langle c_{1(2)\sigma}, c^{\dagger}_{1(2)\sigma}\rangle\rangle^{\mathrm{a}} + \langle\langle c_{2(1)\sigma}, c^{\dagger}_{1(2)\sigma}\rangle\rangle^{\mathrm{a}}\big) \quad (18)$$

$$\langle\langle c_{1(2)\sigma}, a^{\dagger}_{k\sigma}\rangle\rangle^{<} = V^{\mathrm{L}}_{k}\big(\langle\langle c_{1(2)\sigma}, c^{\dagger}_{1(2)\sigma}\rangle\rangle^{\mathrm{r}} + \langle\langle c_{2(1)\sigma}, c^{\dagger}_{1(2)\sigma}\rangle\rangle^{\mathrm{r}}\big) g^{<}_{k} + V^{\mathrm{L}}_{k}\big(\langle\langle c_{1(2)\sigma}, c^{\dagger}_{1(2)\sigma}\rangle\rangle^{<} + \langle\langle c_{2(1)\sigma}, c^{\dagger}_{1(2)\sigma}\rangle\rangle^{<}\big) g^{\mathrm{a}}_{k}. \quad (19)$$

Here $g^{<}_{k} = 2\pi i f_{\mathrm{L}}(\omega)\delta(\omega - \varepsilon^{\mathrm{L}}_{k})$ is the equilibrium distribution GF of the left lead and $f_{\mathrm{L}}(\omega)$ is the Fermi distribution function of the left lead electrons. Since two dots are considered to be symmetric in all respects, each GF of dot-1 looks similar to dot-2. Substitution of the above Dyson equations for the GFs occurring in the current equation, reduces current of the left lead to

$$I_{\mathrm{L}} = -2i\frac{e}{h}\sum_{\sigma}\int \Gamma_{\mathrm{L}}\big[\big(\langle\langle(c_{1\sigma} + c_{2\sigma}), c^{\dagger}_{1\sigma}\rangle\rangle^{<}_{\omega}\big) + f_{\mathrm{L}}\big(\langle\langle c_{1\sigma}, c^{\dagger}_{1\sigma}\rangle\rangle^{\mathrm{r}}_{\omega} - \langle\langle c_{1\sigma}, c^{\dagger}_{1\sigma}\rangle\rangle^{\mathrm{a}}_{\omega}\big) + f_{\mathrm{L}}\big(\langle\langle c_{2\sigma}, c^{\dagger}_{1\sigma}\rangle\rangle^{\mathrm{r}}_{\omega} - \langle\langle c_{2\sigma}, c^{\dagger}_{1\sigma}\rangle\rangle^{\mathrm{a}}_{\omega}\big)\big]\mathrm{d}\omega. \quad (20)$$

Similarly, current due to the right lead can also be written as

$$I_{\mathrm{R}} = -2i\frac{e}{h}\sum_{\sigma}\int \Gamma_{\mathrm{R}}\big[\big(\langle\langle(c_{1\sigma} + c_{2\sigma}), c^{\dagger}_{1\sigma}\rangle\rangle^{<}_{\omega}\big) + f_{\mathrm{R}}\big(\langle\langle c_{1\sigma}, c^{\dagger}_{1\sigma}\rangle\rangle^{\mathrm{r}}_{\omega} - \langle\langle c_{1\sigma}, c^{\dagger}_{1\sigma}\rangle\rangle^{\mathrm{a}}_{\omega}\big) + f_{\mathrm{R}}\big(\langle\langle c_{2\sigma}, c^{\dagger}_{1\sigma}\rangle\rangle^{\mathrm{r}}_{\omega} - \langle\langle c_{2\sigma}, c^{\dagger}_{1\sigma}\rangle\rangle^{\mathrm{a}}_{\omega}\big)\big]\mathrm{d}\omega. \quad (21)$$

If we choose a parameter x such that total current flowing through the system can be written as $I = xI_{\mathrm{L}} - (1-x)I_{\mathrm{R}}$ and $\Gamma_{\mathrm{L}} = \lambda\Gamma_{\mathrm{R}}$ for the so-called proportionate coupling [13,29], where $x = \frac{1}{1+\lambda}$, then the total current can be written as

$$I = \frac{4e}{h}\sum_{\sigma}\int (f_{\mathrm{L}} - f_{\mathrm{R}})\frac{\Gamma_{\mathrm{L}}\Gamma_{\mathrm{R}}}{\Gamma_{\mathrm{L}} + \Gamma_{\mathrm{R}}}\mathrm{Im}\big[\langle\langle c_{1\sigma}, c^{\dagger}_{1\sigma}\rangle\rangle^{\mathrm{r}}_{\omega} + \langle\langle c_{2\sigma}, c^{\dagger}_{1\sigma}\rangle\rangle^{\mathrm{r}}_{\omega}\big]\mathrm{d}\omega$$

$$I = \frac{4e}{h}\sum_{\sigma}\int \big(f_{\mathrm{L}}(\omega) - f_{\mathrm{R}}(\omega)\big)T_{\sigma}(\omega)\mathrm{d}\omega \quad (22)$$

which is similar to the well-known Landauer–Buttiker current formula for transport through mesoscopic systems and derived here for parallel CQD system. Here $T_{\sigma}(\omega)$ is called the transmission coefficient, given by

$$T_{\sigma}(\omega) = \frac{\Gamma_{\mathrm{L}}\Gamma_{\mathrm{R}}}{\Gamma_{\mathrm{L}} + \Gamma_{\mathrm{R}}}\mathrm{Im}\big[\langle\langle c_{1\sigma}, c^{\dagger}_{1\sigma}\rangle\rangle^{\mathrm{r}}_{\omega} + \langle\langle c_{2\sigma}, c^{\dagger}_{1\sigma}\rangle\rangle^{\mathrm{r}}_{\omega}\big]. \quad (23)$$

Also, we can express $\langle\langle c_{2\sigma}, c^{\dagger}_{1\sigma}\rangle\rangle^{\mathrm{r}}$ in terms of $\langle\langle c_{1\sigma}, c^{\dagger}_{1\sigma}\rangle\rangle^{\mathrm{r}}$ as

$$\langle\langle c_{2\sigma}, c^{\dagger}_{1\sigma}\rangle\rangle^{\mathrm{r}}_{\omega} = \left[1 + \langle\langle c_{2\sigma}, c^{\dagger}_{2\sigma}\rangle\rangle^{\mathrm{r}}_{0\omega}\left(V^{*}_{d} - \frac{i}{2}\Gamma\right)\right]\langle\langle c_{1\sigma}, c^{\dagger}_{1\sigma}\rangle\rangle^{\mathrm{r}}_{\omega}. \quad (24)$$

Now, the quantities like I, $T(\omega)$ and differential conductance ($\mathrm{d}I/\mathrm{d}V$), for different Coulomb correlation cases, can be calculated simply by the substitution of the corresponding retarded GF $\langle\langle c_{1\sigma}, c^{\dagger}_{1\sigma}\rangle\rangle^{\mathrm{r}}_{\omega}$ in their respective relations.

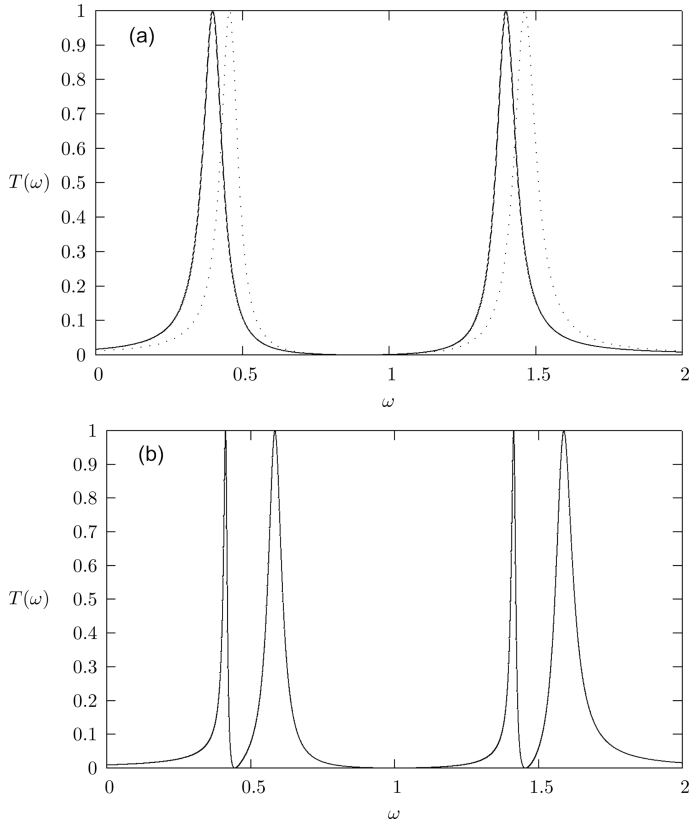

Figure 2. (**a**) The $T(\omega)$ vs. ω graph of parallel CQD at $U = 1$, $\Gamma = 0.08U$ and $\varepsilon = 0.4U$. Solid line denotes $V_d = 0$ and dotted line denotes $V_d = 0.12U$. (**b**) The $T(\omega)$ vs. ω graph of parallel CQD at $U = 1$, $\Gamma = 0.08U$ and $\varepsilon = 0.4U$, $V_d = 0.1U$ and $U' = 0.1U$.

5. Numerical calculations

In this section we present the calculations of transmission coefficient $T(\omega)$, I–V characteristics and differential conductance ($\mathrm{d}I/\mathrm{d}V$). We have considered a perfect symmetric case, in which $\varepsilon_1 = \varepsilon_2 = \varepsilon$, $U_1 = U_2 = U$, $\Gamma_\mathrm{L} = \Gamma_\mathrm{R} = \Gamma/2$ and non-magnetic case such that $\langle n_{i\sigma}\rangle = \langle n_{i\sigma'}\rangle = \frac{1}{2}$. All the parameters have been expressed in units of U. Further, each dot is considered to have single spin degenerate energy level and thus can accommodate a maximum of two electrons with opposite spins. All energies are measured with respect to Fermi level.

5.1 *Transmission coefficient*

The quantity $T(\omega)$ defined in eq. (23), signifies the transmission probability of an electron with energy ω which provides the information of resonant states in

CQD region, participating in electron transport. In case $U' = 0$ and U is finite, $T(\omega) = \frac{\Gamma^2}{\left[(\omega-\varepsilon)(\omega-\varepsilon-U)[\omega-\varepsilon-0.5U]^{-1}-V_d\right]^2+\Gamma^2}$ and is plotted in figure 2a. There are two peaks in the curve, which indicate two resonant energy states possible in each QD. With increase in V_d, the positions of peaks shift towards higher energies roughly by $V_d/2$. Close observations of positions of two peaks reveal that the separation between two resonant states is equal to $U + V_d/20$. This shift might be due to QD level repulsions. The widths of both peaks of $T(\omega)$ are equal to Γ.

Inclusion of U' further changes the energy spectrum of QDs. Although its value is only 10% of U, it has a significant role to play. The transmission coefficient $T(\omega)$ vs. ω, in the presence of both U and U' is plotted in figure 2b. There are four peaks of equal heights (unity), which indicates four resonant energy states possible in CQD, corresponding to energies ε, $\varepsilon+1.5U'$, $\varepsilon+U$ and $\varepsilon+U+1.5U'$. The second and fourth peaks are twice as wide as the first and third, which are calculated to be $\Gamma/3$ and $2\Gamma/3$ respectively.

It is interesting to note that heights of transmission probability resonant peaks are equal to unity in all cases. Hence, symmetric parallel CQD system behaves as an ideal channel for mesoscopic electron transport, irrespective of the values of any CQD parameter. Because of difference in geometry, the situation is entirely different in series CQD system, where channel is reported to be ideal under a specific condition [10,33], i.e. $4V_d^2 = \Gamma_L\Gamma_R$. Moreover, no peak splitting is caused by V_d in parallel CQD while former is the hallmark of the series CQD. Instead, shift in the positions of resonant peaks to higher energies is observed to be the characteristic effect of V_d in parallel CQD. Similar shift has been obtained in ref. [34], but we have found the same in interacting regimes. Further, no Fano effect and splitting of peaks into bonding and antibonding resonances is observed because, equal energies of the resonant levels on both dots and symmetric coupling of CQD to leads, totally decouple the antibonding states from leads and only bonding states participate in electron transport. Therefore, no Fano resonance and splitting can be expected which is observable only in asymmetric parallel CQD case [17,21].

The widths (level broadening) of the $T(\omega)$ vs. ω resonant peaks correspond to the effective coupling of these levels with leads. The width is equal to Γ for each of the two peaks for the case when U is finite and $U' = 0$. In the presence of both types of Coulomb interactions, peaks corresponding to energies ε and $\varepsilon + U$ are of widths $\Gamma/3$ while those at energies $\varepsilon + 1.5U'$ and $\varepsilon + U + 1.5U'$ are of widths $2\Gamma/3$ each, showing that the latter two are effectively more strongly coupled to leads.

5.2 *The V–I characteristics*

In CQD, nature of the V–I graph depends on the kind of arrangement of dots between leads. In the case of CQD in parallel configuration, the V–I graphs are stair-case like structures, similar to those of the SQD system. The step is formed whenever eV matches with the resonant levels on dots. In case $U' = 0$, two steps are observed, while, inclusion of U' adds two small steps to each step observed in $U' = 0$ case. Here the first two steps are clearly visible but the third and fourth are not well resolved (figure 3a). The amount of current (height of I–V step) contributed by any level is proportional to the effective lead–dot coupling coefficient (tunnelling

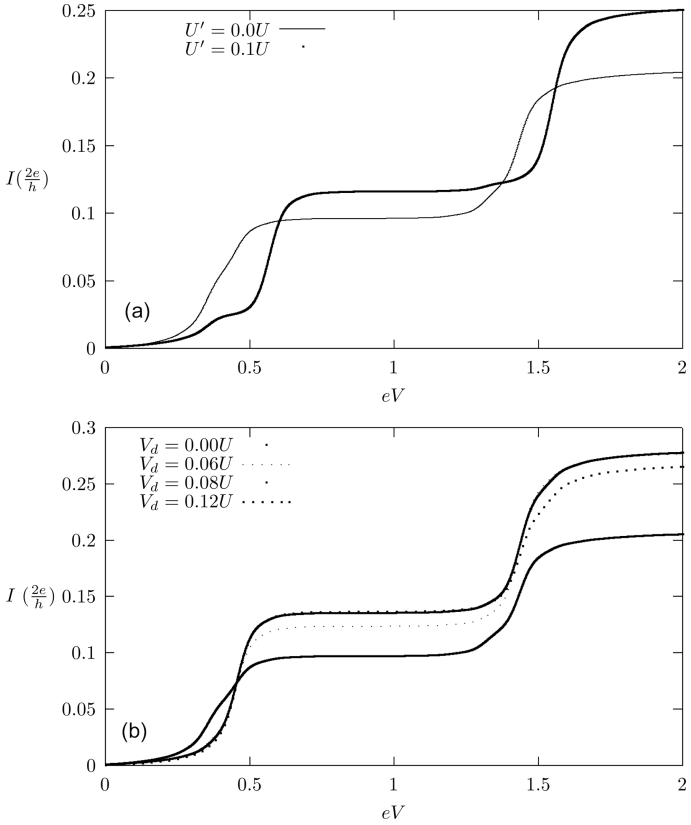

Figure 3. (**a**) The I–V characteristics of parallel CQD at $V_d = 0$, $\Gamma = 0.08U$, $\varepsilon = 0.4U$. Thin line stands for $U' = 0$ and thick line stands for $U' = 0.1U$. (**b**) The I–V characteristics of parallel CQD at different values of V_d at $U = 1$, $\Gamma = 0.08U$, $\varepsilon = 0.4U$. $V_d = 0$ (solid line), $V_d = 0.06U$ (small dotted line), $V_d = 0.08U$ (solid line), $V_d = 0.12U$ (big dotted line).

rate) of that level. But total step heights due to superpositions of current steps at ε and $\varepsilon + 1.5U'$ of lower energy region and $\varepsilon + U$ and $\varepsilon + U + 1.5U'$ of higher energy region in $U' \neq 0$ case, is more than the corresponding step heights at ε and $\varepsilon + U$ in $U' = 0$ case. That means, the presence of U' increases total current through the system because, Coulomb repulsion experienced by electrons from the neighbouring dot decreases inter-dot tunnelling probability and their lifetime on CQD. Thus, electrons are more likely to tunnel to the right lead under the effect of applied bias.

In the case of series CQD system, the V–I graphs show oscillations but in parallel CQD, graphs show stair-case structure hence behave more or less similar to single QD system. In fact, in parallel CQD (figure 1), there are multiple pathways possible for electron transport, viz. $L \to D_1 \to R, L \to D_2 \to R, L \to D_1 \to D_2 \to R$ and $L \to D_2 \to D_1 \to R$ are primarily more probable ones, while there can be a small possibility of two more paths: $L \to D_1 \to D_2 \to D_1 \to R$ and $L \to D_2 \to D_1 \to$

$D_2 \rightarrow R$. Total current is the quantum-mechanical superposition of all the currents, although dominant contribution is from the first two paths which form two single QD systems. As a result I–V characteristics of parallel CQDs are similar to SQD systems. In contrast to this, series CQD system has only one path available for electron transport.

Here it will be interesting to see the role of V_d, which directly influences the probability of selection of one of the above-mentioned paths by electrons, in parallel CQD. In case two dots are decoupled from each other ($V_d = 0$), current will be solely due to the first two paths. As the coupling between two dots is introduced, third and fourth paths show their effects. With increase in V_d, total current through the system increases, i.e. heights of steps in the I–V graph increase and show saturation when inter-dot coupling approaches Γ (figure 3b). At this condition two dots merge to form a big single QD. For $V_d > \Gamma$, the total current starts decreasing.

5.3 *Differential conductance* ($\mathrm{d}I/\mathrm{d}V$)

To calculate differential conductance, eq. (22) is differentiated with respect to V. Due to different chemical potentials of the two leads, the electron tunnelling occurs whenever difference in electron chemical potentials of leads matches with the resonant levels of CQD shown in $T(\omega)$ vs. ω curves. Thus differential conductance also reveals various resonant levels present in the CQD system under non-equilibrium condition. Also, at low temperature it is difficult to align different resonant levels of both the dots, resulting in splitting of each resonant peak. If temperature is increased, no splitting is observed (figure 4a), showing proper alignment of resonant levels of two dots with each other.

If U' is neglected but U is taken into account, the latter dominates all other parameters, i.e. $U \gg [V_d, \Gamma, \varepsilon]$. When $V_d = 0$, we get two sets of differential conductance peaks displayed around ε and $\varepsilon + U$, each of which is split into two unresolved peaks, i.e. four peaks of unequal heights are displayed corresponding to the two resonant peaks contributed by each dot. Each of these peaks behaves differently for various values of V_d. Figures 4a–f show the differential conductance spectra of CQD for various values of V_d. On increasing V_d, heights of the first and third peaks decrease monotonously, while second and fourth peaks show increase in their heights upto the point when V_d becomes equal to Γ and decrease beyond that. Interestingly, at $V_d = \Gamma$, four peak structures merge into two peaks of average height equal to unitary limit of conductance $2e^2/h$ (figure 4c), which again gives the indication of merger of two dots into a single big QD. The phenomena of merger of two dots with inter-dot coupling has been reported in many experimental work on parallel CQD [18,19] and theoretically in series CQD [35].

The increase in V_d beyond Γ generates more secondary peaks to the right sides of both the peaks. In case V_d approaches 3Γ, physical behaviour of the system resembles that of two decoupled dots ($V_d = 0$) (figure 4f). Similar behaviour was observed by the authors of refs [4,18]. But there is no simple explanation for this kind of behaviour of secondary peaks.

The behaviour of conductance peaks for varying V_d is different in series and parallel CQD systems. In series case the separations between two peaks of each

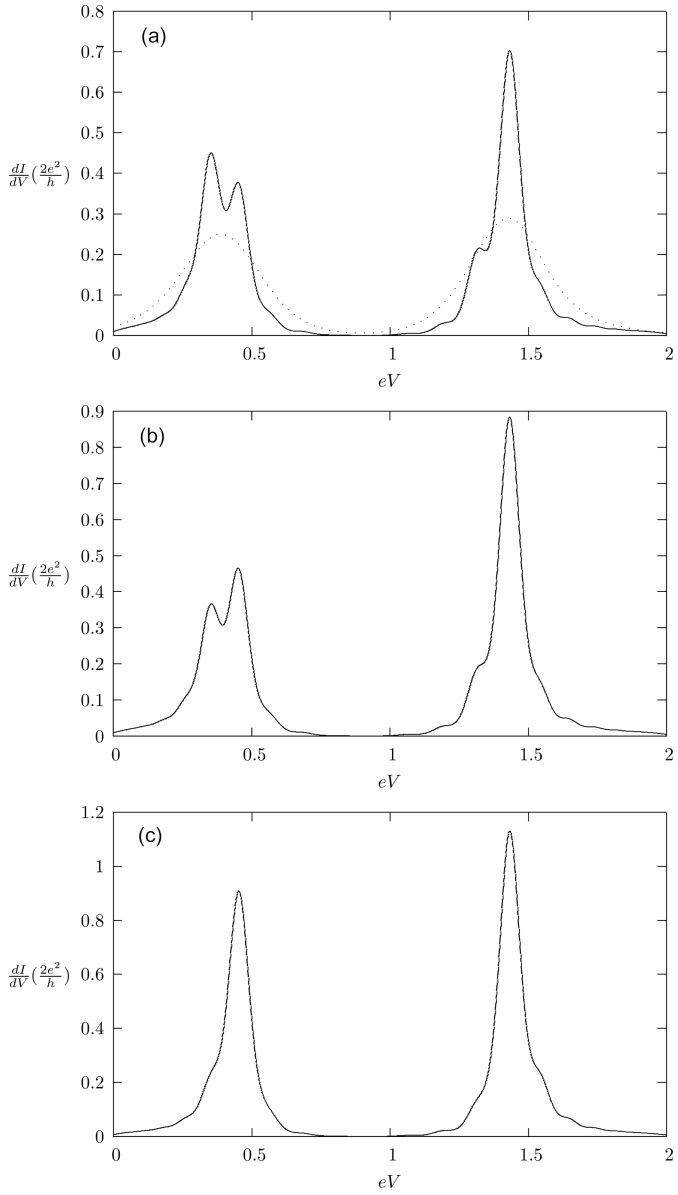

Figure 4. (**a**) The differential conductance vs. bias voltage graph of parallel CQD at $U = 1$, $\Gamma = 0.08U$, $\varepsilon = 0.4U$ and $V_d = 0$. Solid line stands for $kT = 0.025U$ and dotted line stands for $kT = 0.075U$. (**b**) The differential conductance vs. bias voltage graph of parallel CQD at $U = 1$, $\Gamma = 0.08U$, $\varepsilon = 0.4U$, $kT = 0.025U$ and $V_d = 0.02U$. (**c**) The differential conductance vs. bias voltage graph of parallel CQD at $U = 1$, $\Gamma = 0.08U$, $\varepsilon = 0.4U$, $kT = 0.025U$ and $V_d = 0.08U$.

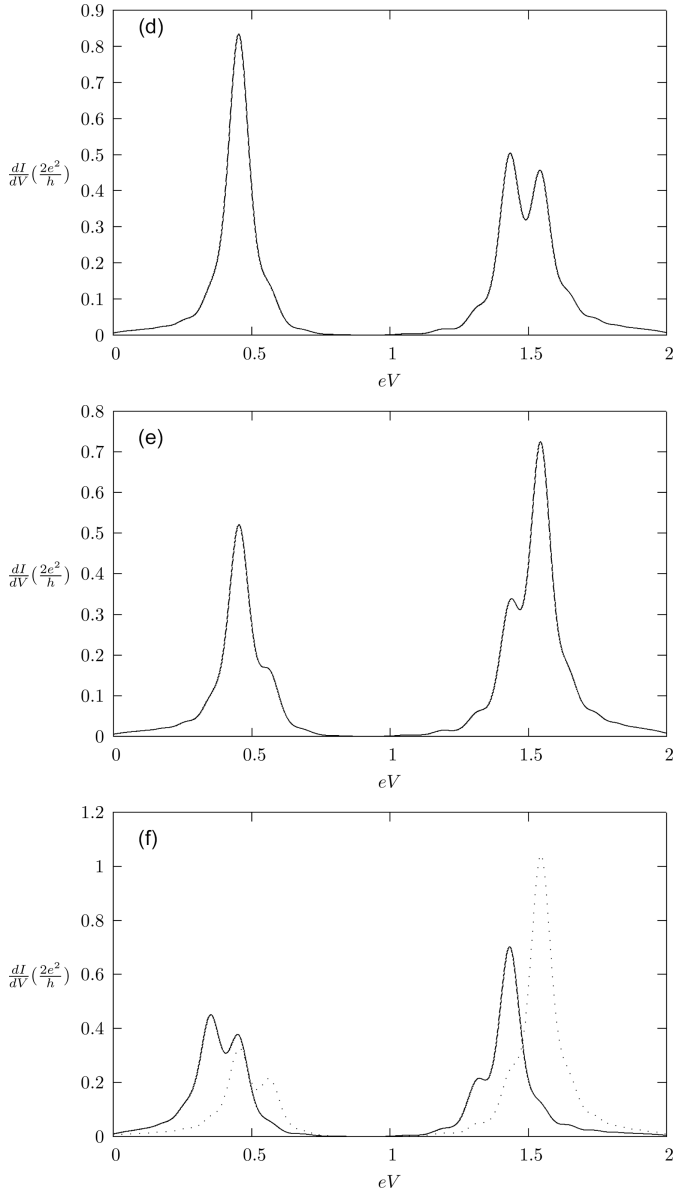

Figure 4. (**d**) The differential conductance vs. bias voltage graph of parallel CQD at $U = 1$, $\Gamma = 0.08U$, $\varepsilon = 0.4U$, $kT = 0.025U$ and $V_d = 0.16U$. (**e**) The differential conductance vs. bias voltage graph of parallel CQD at $U = 1$, $\Gamma = 0.08U$, $\varepsilon = 0.4U$, $kT = 0.025U$ and $V_d = 0.2U$. (**f**) The differential conductance vs. bias voltage graph of parallel CQD at $U = 1$, $\Gamma = 0.08U$, $\varepsilon = 0.4U$ and $kT = 0.025U$. Solid lines stands for $V_d = 0U$ and dotted line stands for $V_d = 0.24U$.

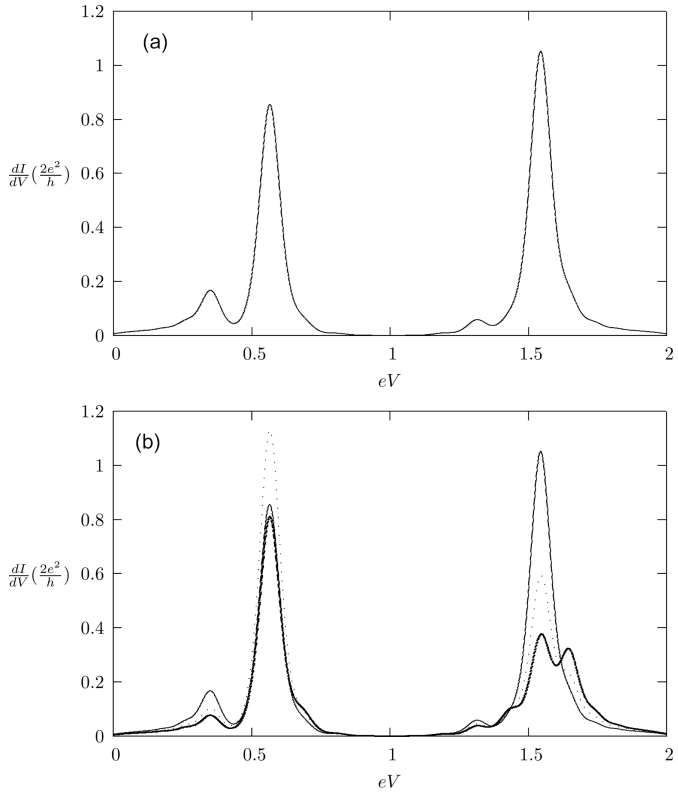

Figure 5. (**a**) The differential conductance as a function of eV of parallel CQD at $U = 1$, $U' = 0.1U$, $\Gamma = 0.08U$, $\varepsilon = 0.4U$, $kT = 0.025U$ and $V_d = 0$. (**b**) The differential conductance vs. bias voltage of parallel CQD at $U = 1$, $U' = 0.1U$, $\Gamma = 0.08U$ and $\varepsilon = 0.4U$. Thin line stands for $V_d = 0$, thick dotted line stands for $V_d = 0.06U$ and thick line stands for $V_d = 0.1U$.

set of peaks increase with increase in V_d and saturates when two dots merge to form a big composite dot [35]. But no such separation is observed in the parallel case wherein four peaks merge to form two peaks. Also, in the case of series CQD, Coulomb blockade may lead to negative differential conductance. But negative differential conductance is not observed in symmetric parallel CQD.

Further, we calculate $\mathrm{d}I/\mathrm{d}V$ in the presence of U' (figure 5a,b). The noticeable change in the differential conductance peaks is that the positions of the first and third resonant peaks do not change while the second and fourth peaks shift to higher energy values by $1.5U'$, showing many-body effects. There is an interesting interplay between U' and V_d in the system which is reflected in the $\mathrm{d}I/\mathrm{d}V$ vs. eV curves for various values of V_d. In both sets of peaks, the first and third peaks decrease continuously with V_d, while the second peak grows in height upto the point when $V_d = U'$ and decreases beyond that continuously. But fourth peak shows monotonous decrease. However, secondary peak structure is generated to the right of the fourth peak, which shows increase in height with increase in V_d.

6. Conclusions

In the present work we investigated the non-equilibrium transport properties of symmetric parallel CQD system, in Coulomb blockade regime, in the presence of inter-dot and intra-dot Coulomb correlations among electron, using NEGF approach. We derived the transport observables in terms of Green functions of dots. Summary of conclusions drawn from the present work is as follows:

- The $T(\omega)$–ω curves show that there are two energy levels of the system at ε and $\varepsilon + U$ in $U' = 0$ case and four energy levels with energies ε, $\varepsilon + 1.5U'$, $\varepsilon + U$ and $\varepsilon + U + 1.5U'$ in the presence of U' which participate in electron transport.
- Heights of $T(\omega)$–ω resonant peaks are always unity. Therefore, symmetric parallel CQD behaves as an ideal channel for the electron transport.
- The I–V characteristics of parallel CQD system resemble the SQD system, having stair-case like steps in both the systems. The number and heights of steps are strongly influenced by the Coulomb correlations.
- The presence of inter-dot Coulomb correlation increases the overall current through the CQD system as compared to only intra-dot Coulomb case.
- In case $U' = 0$ and for weak coupling regime $V_d < \Gamma$, initially current starts increasing and saturates when V_d approaches Γ and at this stage four conductance peaks merge to form two peaks. This gives a clear indication of merger of two dots into a big single composite dot.
- For strong coupling case ($V_d > \Gamma$) current starts decreasing and secondary peaks are observed in $\mathrm{d}I/\mathrm{d}V$ spectrum and for large coupling, physical behaviour in conductance spectrum resembles the decoupled dots ($V_d = 0$).
- Negative differential conductance, observed in series CQD, is not reported in symmetric parallel CQD.
- The comparison with the results of refs [10,11] (where magnitudes of parameters is nearly similar to the present work) reveals that the total current and conductance of symmetric parallel CQD is much larger than in series CQD system.

References

[1] T Aonu and M Eto, *Phys. Rev.* **B63**, 125327 (2001)
[2] W Izumida and O Sakai, *Phys. Rev.* **B62**, 10260 (2000)
[3] A Georges and Y Meir, *Phys. Rev. Lett.* **82**, 3508 (1999)
[4] R Aguado and D C Langreth, *Phys. Rev. Lett.* **85**, 1946 (2000)
[5] M A Kastner, *Rev. Mod. Phys.* **64**, 849 (1992)
[6] H Grabert and M H Devoret, *Single charge tunneling* (Plenum Press, New York, 1992)
[7] P Mehta and N Andrei, *Phys. Rev. Lett.* **96**, 216802 (2006)
[8] A Dhar, D Sen and D Roy, *Phys. Rev. Lett.* **101**, 066805 (2008)
[9] D Loss and D P DiVincenzo, *Phys. Rev.* **A57**, 120 (1998)
[10] Chang Niu, Li-jun Liu and Tsung-han Lin, *Phys. Rev.* **B51**, 5130 (1995)

[11] Sushil Lamba and S K Joshi, *Phys. Rev.* **B62**, 1580 (2000)
[12] J Q You and H Z Zheng, *Phys. Rev.* **B60**, 8727 (1999)
[13] L G Mourokh, N J M Horing and A Y Smirnov, *Phys. Rev.* **B66**, 085332 (2002)
[14] D Loss and E V Sukhorukov, *Phys. Rev. Lett.* **84**, 1035 (2000)
[15] D Boese, W Hofstetter and H Shoeller, *Phys. Rev.* **B64**, 125315 (2002)
[16] K Kang and S Y Cho, *J. Phys. Condens. Matter* **16**, 117 (2004)
[17] M L Ladron de Guevara, F Claro and P A Orellana, *Phys. Rev.* **B67**, 195335 (2003)
[18] A S Adourian, C Livermore and R M Westervelt, *Appl. Phys. Lett.* **75**, 424 (1999)
[19] J C Chen, A M Chang and M R Melloch, *Phys. Rev. Lett.* **92**, 176801 (2004)
[20] Tae-Suk Kim and S Hershfield, *Phys. Rev.* **B63**, 245326 (2001)
[21] Rong Lu, Zhi-Rong Liu and G Ming Zhang, cond-mat/0504288 v1 (2005)
[22] H Lu, Rong Lu and Bang-fen Zhu, cond-mat/0511101 v1 (2005)
[23] Feng Chi and Shu-Shen Li, *J. Appl. Phys.* **99**, 043705 (2006)
[24] Feng Chi and Shu-Shen Li, *J. Appl. Phys.* **97**, 123704 (2005)
[25] P W Anderson, *Phys. Rev.* **124**, 41 (1961)
[26] L V Keldysh, *Zh. Eksp. Teor. Fiz.* **47**, 1515 (1964) [*Sov. Phys. JETP* **20**, 1018 (1965)]
[27] L P Kadanoff and G Baym, *Quantum statistical mechanics* (Benjamin, New York, 1962)
G D Mahan, *Phys. Rep. (Rev. Section Lett.)* **145**, 251 (1987)
[28] C Caroli, R Combescot, P Nozieres and D Saint-James, *J. Phys.* **C4**, 916 (1971)
[29] A P Jouho, N S Wingreen and Y Meir, *Phys. Rev.* **B50**, 5528 (1994)
Y Meir and N S Wingreen, *Phys. Rev. Lett.* **68**, 2512 (1992)
N S Wingreen and Y Meir, *Phys. Rev.* **B49**, 11040 (1994)
[30] C Lacroix, *J. Phys.* **F11**, 2389 (1981)
[31] D N Zubarev, *Usp. Fiz. Nauk* **71**, 71 (1960) [*Sov. Phys. Usp.* **3**, 320 (1960)]
[32] D C Langreth, in: *Linear and nonlinear electron transport in solids*, Vol. 17, Nato Advanced Study Institute, Series B: Physics, edited by J T Devreese and V E Van Doren (Plenum, New York, 1976)
[33] A I Larkin and K A Matveev, Zh. Eksp. Teor. Fix. **93**, 1030 (1987) [*Sov. Phys. JETP* **66**, 580 (1987)]
[34] Guo-Hui Ding, C K Kim and Kyun Nahm, cond-mat/0412502 v2 (2005)
[35] F R Waugh, M J Berry, D J Mar, R M Westervelt, K L Campman and A C Gossard, *Phys. Rev.* **B53**, 1413 (1996)